


Article

Simulating Evaluation Method on Heating Performances of Magnetic Nanoparticles with Temperature-Dependent Heating Efficiencies in Tumor Hyperthermia

Shuai-Wen Ding¹, Cheng-Wei Wu¹, Xiao-Gang Yu¹, Chao Dai¹, Wei Zhang^{1,*}  and Jian-Po Gong²

¹ State Key Laboratory of Structural Analysis for Industrial Equipment, Department of Engineering Mechanics, Dalian University of Technology, Dalian 116024, China; bddingsw@163.com (S.-W.D.); cwwu@dlut.edu.cn (C.-W.W.); yxg@dlut.edu.cn (X.-G.Y.); dc1997@mail.dlut.edu.cn (C.D.)

² Weichai Ballard Hy-Energy Technologies Co., Ltd., Weifang 261061, China; gongjp@weichai.com

* Correspondence: wei.zhang@dlut.edu.cn

Abstract: The magnetic nanoparticles (MNPs) with decreasing heating efficiency (characterized by specific loss power, *SLP*) with temperature increase, especially around the Curie temperature (T_C), are expected to realize the self-regulated temperature hyperthermia of the tumor. However, the actual decrease of the *SLP* is gradual, resulting in the deviation of self-regulated temperatures from the measured T_C . So far, no method is available for evaluating the heating performances of those MNPs. Here, by simulating the temperature-dependent *SLP*, the heating performances of MNPs are evaluated from three clinically concerning aspects: the capacity for effective heating, the temperature uniformity in the tumor, and the temperature stability under environmental changes such as MNP loss or tumor progression. The developed methods were applied to ZnCoCrFeO, Fe₃O₄, and γ -Fe₂O₃ MNPs. It was found that the uniform temperature distribution relies on lowering the heating power in the inner regions of the tumor, and the stable control of temperature depends on the dynamic adaptation of the heating power to the tumor temperature change. The proposed method may be used to predict the heating ability of MNPs and help the selection of MNPs for hyperthermia.

Keywords: magnetic nanomaterial; magnetic nanoparticle; self-regulating temperature; hyperthermia; numerical simulation



Citation: Ding, S.-W.; Wu, C.-W.; Yu, X.-G.; Dai, C.; Zhang, W.; Gong, J.-P. Simulating Evaluation Method on Heating Performances of Magnetic Nanoparticles with Temperature-Dependent Heating Efficiencies in Tumor Hyperthermia.

Magnetochemistry **2022**, *8*, 63.

<https://doi.org/10.3390/magnetochemistry8060063>

magnetochemistry8060063

Academic Editor: Lotfi Bessais

Received: 8 April 2022

Accepted: 28 April 2022

Published: 8 June 2022

Publisher's Note: MDPI stays neutral with regard to jurisdictional claims in published maps and institutional affiliations.



Copyright: © 2022 by the authors. Licensee MDPI, Basel, Switzerland. This article is an open access article distributed under the terms and conditions of the Creative Commons Attribution (CC BY) license (<https://creativecommons.org/licenses/by/4.0/>).

1. Introduction

After being introduced to tumors, magnetic nanoparticles (MNPs) can heat and cure tumors under an alternating magnetic field (AMF) with few side effects. The efficiency of the therapy has been verified in several clinical trials [1–4]. For further improving the therapeutic effects, the MNPs with suitable Curie temperature (T_C) attracted attention for better temperature control [5]. The T_C is the critical temperature at which the MNPs transform from ferromagnetic to paramagnetic and lose heating abilities under AMF. By selecting the MNPs with proper T_C , the temperature in the tumor can be self-regulated at preferred temperature ranges of different therapies, removing the burdens of thermometers and cooling systems [5]. In addition, these MNPs can produce uniform temperature distribution all over the tumor and lead to consistent therapeutic outcomes [6,7]. By now, MNPs with T_C of 37–93 °C have been manufactured. Their ability to self-regulate temperatures has been verified both in vitro [8–10] and in vivo [11–14].

In previous work, we reported ZnCoCrFeO MNPs with T_C of 29–103 °C [10]. The ZnCoCrFeO MNPs with T_C of 61 °C could self-regulate temperatures at 43–44 °C in vivo [14]. The MnZnFeO ferrite MNPs with T_C of 89.6 °C raised the temperature of tumors in nude mice to 42.8 °C [11]. However, the ZnCoCrFeO MNPs with T_C of 37.5 °C elevated the water temperature to 43.8 °C [10]. Similarly, the FeCuZnMgO ferromagnetic MNPs with T_C of 43 °C achieved 45 °C in vivo [13]. The ZnFeO MNPs with T_C of 93 °C obtained

41.5 °C in cellular magnetic heating experiments [9]. Clearly, the deviations exist between T_C and self-regulated temperature, suggesting the insufficiency of using T_C to predict the heating performances of MNPs. Theoretically, the ideal MNPs should have high heating efficiency (represented by specific loss power, SLP) below T_C , and the SLP instantly drops to zero at T_C . Thus, the temperature can be controlled at T_C . However, the actual decline of SLP around T_C is usually gradual, leaving residual SLP and extra heating abilities over T_C [14]. It seems necessary to consider the temperature-dependent SLP for predicting the heating abilities, rather than just relying on the T_C and a single SLP value. However, no such evaluation standard can be found yet.

In this paper, a tumor simulation model considering the temperature-dependent SLP was established to predict the heating capacity of MNPs in hyperthermia and their performances in forming a uniform and stable temperature distribution in the tumor. The method was applied to 46 °C hyperthermia of ZnCoCrFeO [14], Fe₃O₄ [15,16] and γ -Fe₂O₃ MNPs [17]. It was found that the MNPs with a steeper decrease of heat source power densities within 37–46 °C can reduce the heating power in the inner tumor regions and automatically adjust the heating power to the tumor temperature changes, possessing better uniformities and stabilities.

2. Materials and Methods

2.1. Temperature-Dependent SLP Measurements

The MNPs were manufactured by the methods used in previous studies [10,14]. The Zn_{0.54}Co_{0.46}Cr_{0.7}Fe_{1.3}O₄, Zn_{0.54}Co_{0.46}Cr_{0.65}Fe_{1.35}O₄ and Zn_{0.54}Co_{0.46}Cr_{0.6}Fe_{1.4}O₄ MNPs with T_C of 37.5 °C, 56.0 °C and 61.0 °C are signed as MNP₃₇, MNP₅₆, and MNP₆₁. The SLP data were calculated, based on the temperature-time (T - t) data from the calorimetry experiments. The experimental setup (Figure 1a) is as follows. The MNPs were fixed by hydrogel in a tube as magnetic hydrogel (MHG) for uniform and stable dispersion [14]. The tube was placed in a Dewar vacuum flask for reducing heat dissipation. Then, they were surrounded by circulating water with controllable temperature. The fiber optic thermometer (Fotemp-Trafo FTT-0100, Optocon, Dresden, Germany) monitored the central temperature of 2 mL MHG of 80 mg/mL (MNPs mass/hydrogel volume) in the tube. Before calorimetry measurements, the inner startup temperatures were monitored by the fiber optic thermometer and controlled by adjusting the circulating water temperature. When the startup temperatures were stable, the AMF generator (GUF-30T, Shenqiu Yongda High Frequency Equipment Co., Ltd., Zhoukou, China) heated the MNPs at 400 ± 5 Oe and 100 ± 5 kHz for 3 min to obtain the T - t curves. The startup temperatures were set from 20 °C to 75 °C with a 5 °C interval. The measurement was repeated four times for each kind of MNPs at each startup temperature. The mean values of T - t curves were used for the calculations of SLP data.

The SLP describes the heat, converted from the energy of AMF, per unit time and unit MNP mass, as Equation (1) [18].

$$SLP = c_{\text{MHG}} \times \left(\frac{dT}{dt} \right) \times \left(\frac{m_{\text{MHG}}}{m_{\text{MNP}}} \right) \quad (1)$$

where, c_{MHG} is the specific heat capacity of MHG (2.30 ± 0.18 J/(g·°C)) [14]; T is the temperature (°C); t is the time (s); dT/dt is the initial slope of the T - t curve (the linear fragment at 10–20 s of temperature rising), provided the temperature distribution within the sample is homogeneous and the initial thermal losses are negligible [19,20]; m_{MHG} is the mass of MHG (mg); m_{MNP} is the mass of MNPs (mg). The T - t data and SLP data of MNP₆₁ were cited from reference [14].

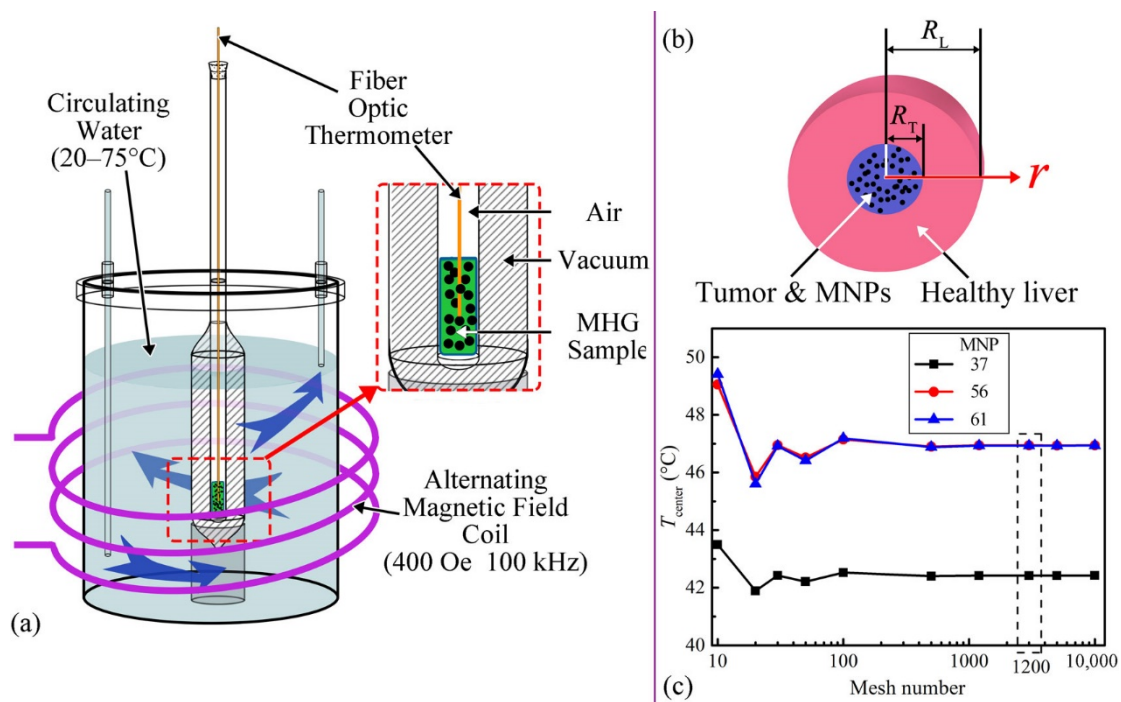


Figure 1. (a) Experimental setup of calorimetry experiments; (b) Tissue model of the thermal simulations, R_T is the radius of the sphere tumor, R_L is the radius of the healthy liver tissue; (c) Convergence analysis of mesh number about the final temperatures of tumor center (T_{center}), with 1200 as the chosen mesh number.

2.2. Heating Performance Simulations

The model is shown in Figure 1b, i.e., a sphere tumor (15 mm radius) surrounded by healthy liver tissue (90 mm radius). The MNPs were assumed to be evenly distributed in the tumor without displacement and loss. Two Pennes bioheat transfer equations for simulating the temperature changes in tumor and healthy tissue are as Equations (2) and (3) [21].

$$\rho_{TP}c_{TP} \frac{\partial T(r,t)}{\partial t} = \frac{k_{TP}}{r^2} \frac{\partial \left(r^2 \frac{\partial T(r,t)}{\partial r} \right)}{\partial r} + Q_{mT}(T) + Q_{bT}(T) + PDP(T) \quad (0 < r < R_T) \quad (2)$$

$$\rho_{LC}c_{LC} \frac{\partial T(r,t)}{\partial t} = \frac{k_L}{r^2} \frac{\partial \left(r^2 \frac{\partial T(r,t)}{\partial r} \right)}{\partial r} + Q_{mL}(T) + Q_{bL}(T) \quad (R_T < r < R_L) \quad (3)$$

The initial condition is as Equation (4).

$$T(r,0) = 37 \text{ }^\circ\text{C} \quad (4)$$

At the interface of the tumor and healthy tissue, the temperature and heat flow are continuous. In addition, the inner and outer boundary conditions are as Equations (5) and (6).

$$\left. \frac{\partial T(r,t)}{\partial r} \right|_{r=0} = 0 \quad (5)$$

$$T(r,t)|_{r=R_L} = 37 \text{ }^\circ\text{C} \quad (6)$$

where, T is the temperature (°C); r is the radius from the center (m); R_T is the radius of the tumor (15 mm); R_L is the radius of healthy liver tissue (90 mm); ρ is the density (kg/m³); c is the specific heat capacity (J/(kg·°C)); k is the thermal conductivity (W/(m·°C)); Q_m is the power density of metabolic heat generation (W/m³); Q_b is the power density of heat dissipation by blood perfusion effect (W/m³); PDP is the power density of MNPs [7], i.e.,

the power dissipation of MNPs per unit of volume (W/m^3); the subscript T represents the tumor; the subscript L represents the healthy liver tissue; the subscript TP represents the tumor region with evenly distributed MNPs. The ρ , c , and k of the tumor region change with the MNP concentration as Equation (7) [22,23].

$$\begin{cases} \rho_{TP} = (1 - \phi)\rho_T + \phi\rho_P \\ c_{TP} = (1 - \phi)c_T + \phi c_P \\ \frac{1}{k_{TP}} = \frac{(1 - \phi)}{k_T} + \frac{\phi}{k_P} \end{cases} \quad (7)$$

where, the subscript P represents MNPs; ϕ is the volume fraction of MNPs in the tumor, which can be calculated through $\phi = C/\rho_P$; and the C is the concentration of MNPs in the tumor (kg/m^3 or mg/mL , MNP mass/tumor volume).

The Q_m and Q_b rely on the body temperature change. The Q_m (W/m^3) is as Equation (8) [24].

$$Q_m(T) = Q_{m0}[1 + 0.1(T - 37)] \quad (8)$$

where, Q_{m0} is the Q_m when the tissue is at $37^\circ C$ (W/m^3).

The Q_b (W/m^3) is as Equation (9) [25].

$$Q_b(T) = w_b\rho_b c_b \times (T_\alpha - T) \quad (9)$$

where, the subscript b represents blood; w_b is the blood perfusion rate ($1/s$); T_α is the temperature of arterial blood ($^\circ C$), here assumed as $37^\circ C$.

The physical parameters used for tissues and MNPs are shown in Table 1.

Table 1. Physical parameters of tissues and MNPs.

	ρ kg/m^3	c $J/(kg \cdot ^\circ C)$	k $W/(m \cdot ^\circ C)$	w_b $1/s$	Q_{m0} W/m^3
Tumor [7]	1060	3540	0.52	0.000833	5790
Blood [26]	1050	3617	N/A	N/A	N/A
Liver [26]	1079	3540	0.52	0.0155	10,682
MNPs [7]	5180	670	40	N/A	N/A

The $PDP(T)$ is calculated as Equation (10) [27].

$$PDP(T) = SLP(T) \times C \quad (10)$$

where, $SLP(T)$ is the specific loss power of MNPs (W/kg), obtained in the experiments; C is the MNP concentration (kg/m^3 , MNP mass/tumor volume).

The Pennes bioheat transfer equations were solved by the PDEPE function in MATLAB. The mesh numbers of time and spatial dimensions were equal. The convergence of mesh numbers was analyzed by comparing the final temperatures of the tumor center at different mesh numbers in Figure 1c. The MNP concentration in the convergence analysis was $35 mg/mL$. The mesh number of 1200 was selected.

3. Results and Discussion

3.1. SLP-T Relationships

The temperature-time ($T-t$) curves of the MHG of ZnCoCrFeO MNPs are shown in Figure 2a–c. As the startup temperature increases, the temperature rising amplitude gradually decreases to zero, indicating that the MNPs have self-regulating temperatures. However, the elevated temperatures can exceed the T_C , indicating that the MNPs have residual heating abilities over T_C . The initial slopes of the $T-t$ curves are extracted for SLP calculations (Equation (1)). In addition, the $SLPs$ at different temperatures are shown in Figure 2d. With the increase of temperature, the SLP decreases gradually around

the T_C , ranging for dozens of degrees. Above the T_C , considerable residual SLP exists, possibly resulting from the underestimated T_C by measurement methods. The T_C is normally determined by locating the maximum first derivatives of the thermogravimetric mass-temperature curves [10,14] or the minimum first derivatives of the magnetization-temperature curves [8]. So, the obtained T_C value represents the majority of the MNPs. While the MNPs, in fact, always have a wide range of T_C (some over 100 °C [10,14]). The measurement methods are practical for determining the representative T_C but may result in inaccurate prediction of heating performances. For accurate predictions, the $SLPs$ at different temperatures should be considered. The $SLP-T$ data were fitted with Gaussian curves to provide the heat source in simulations with continuous coupling relationships. The fitting equation is as Equation (11).

$$SLP(T) = a \times e^{-(\frac{T-b}{c})^2} \tag{11}$$

where, a , b and c are the fitting parameters, summarized in Table 2.

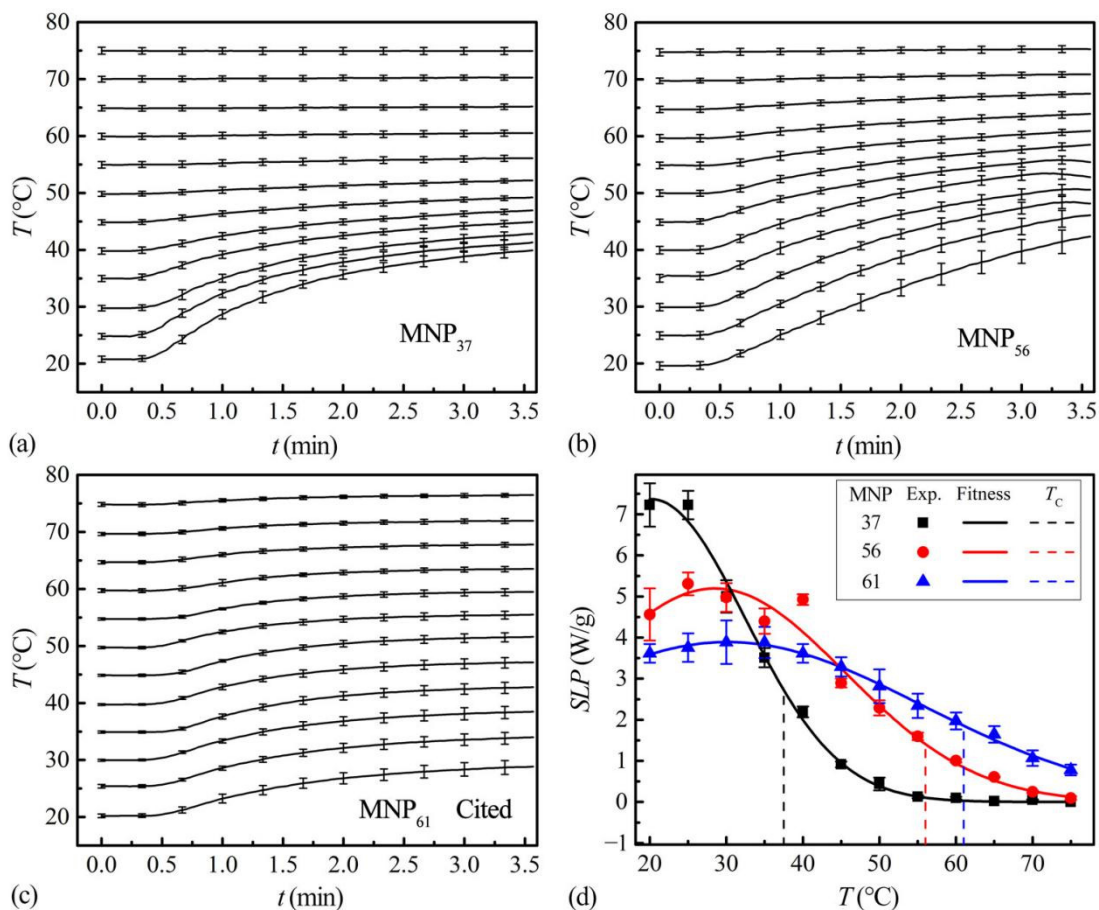


Figure 2. The $T-t$ data of the MNP_{37} (a), MNP_{56} (b), and MNP_{61} from reference [14] (c) at different initial temperatures (20–75 °C, 5 °C intervals); $n = 4$ for each line, data: mean value and standard uncertainty. (d) Experimental SLP data and fitted $SLP-T$ curves of MNP_{37} , MNP_{56} and MNP_{61} ; the SLP data of MNP_{61} were from reference [14]; $n = 4$ for each point, data: mean value and standard uncertainty.

Table 2. Gaussian fitting parameters of $SLP-T$ curves for ZnCoCrFeO MNPs.

	a	b	c
MNP_{37}	7.369	20.210	17.330
MNP_{56}	5.196	28.500	24.070
MNP_{61}	3.892	30.200	35.770

3.2. Heating Performances

3.2.1. Temperature Rises and Distributions

The temperature changes in time and spatial dimensions of the three ZnCoCrFeO MNPs are shown in Figure 3a–c. In addition, the corresponding temperature rises of tumor centers and the final temperature distributions are summarized in Figure 3d. The temperatures rise from 37 °C (body temperature). So, the SLP over 37 °C (Figure 2d) contributes to the heating processes and should be focused on. The temperature increase in the tumor stops after about 10 min, which can be seen from the central temperatures in Figure 3d (lower abscissa). Furthermore, the final temperature distributions, in Figure 3d (upper abscissa), would last for another 50 min in the one-hour clinical hyperthermia treatment, mainly determining the curing effects [1–4]. Thus, in the following heating performance evaluations, the final temperature distributions would be focused on. In the tumor, the maximum and minimum temperatures appear at the center and the edge, marked in Figure 3d. So, the final temperatures at the center (T_{center}) and the edge (T_{edge}) would be used to represent the final temperature range within the tumor in the simulations hereafter.

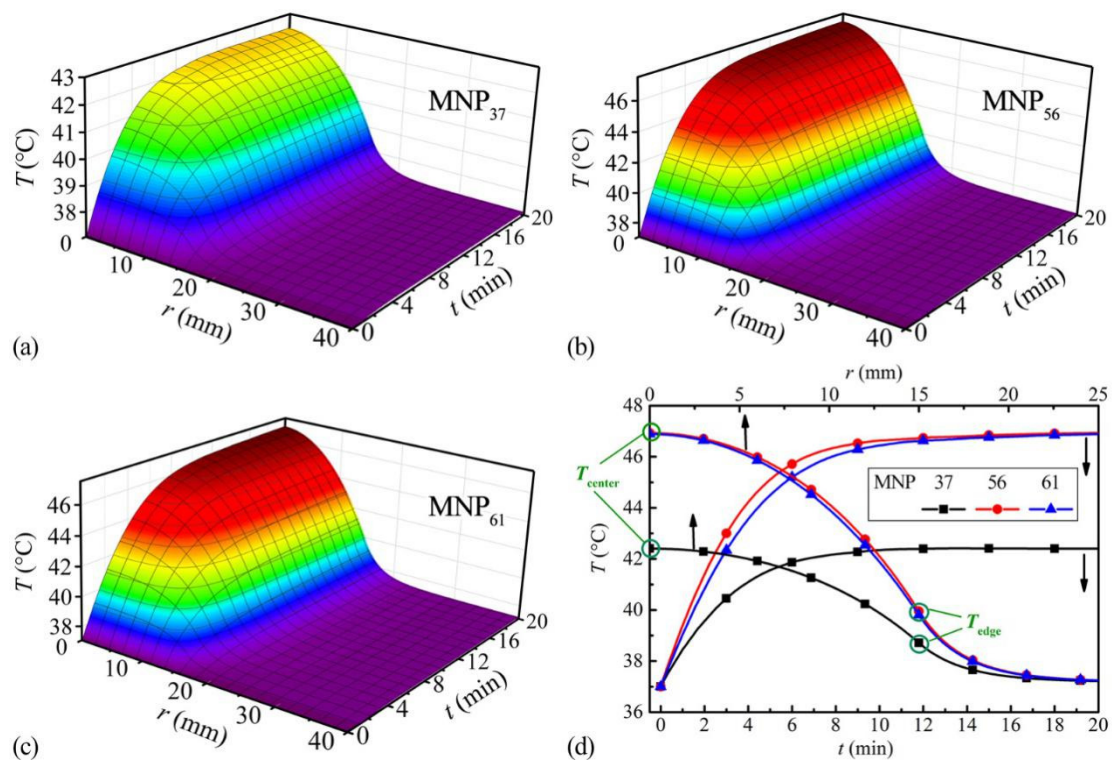


Figure 3. The time and spatial temperature changes in the tissue model of MNP₃₇ (a), MNP₅₆ (b) and MNP₆₁ (c), at 35 mg/mL MNP concentration; (d) The corresponding temperature rises of tumor centers (lower abscissa) and the final temperature distributions (upper abscissa).

In the following simulations of heating performances, three kinds of MNPs in references with temperature-dependent SLP (T_C unknown) are also included. They are signed after the authors' names as MNP_{Nemala} (Fe_3O_4) [15], MNP_{Regmi} (Fe_3O_4) [16], and MNP_{Beković} ($\gamma\text{-Fe}_2\text{O}_3$) [17]. The SLP data, extracted from references [15–17], are shown in Figure 4a. They are fitted by Equation (11) for the curves in Figure 4a. Furthermore, the fitting parameters are shown in Table 3. In addition, two assumed MNPs are also simulated, in order to exhibit the improvements and limitations in heating performances of the actual MNPs. They are the MNPs without T_C (MNP_{none}) with the SLP of 6 W/g at any temperature, and the ideal MNPs (T_C 46 °C, MNP_{ideal}) with the SLP of 6 W/g under T_C and 0 W/g above T_C . The chosen 6 W/g is within the 5–7 W/g of MNP₅₆ and MNP₃₇.

For convergence consideration, the SLP decrease of MNP_{ideal} was set as a linear drop from 6 W/g at 45.99 °C to 0 W/g at 46.00 °C. Their SLP - T curves are shown in Figure 4b.

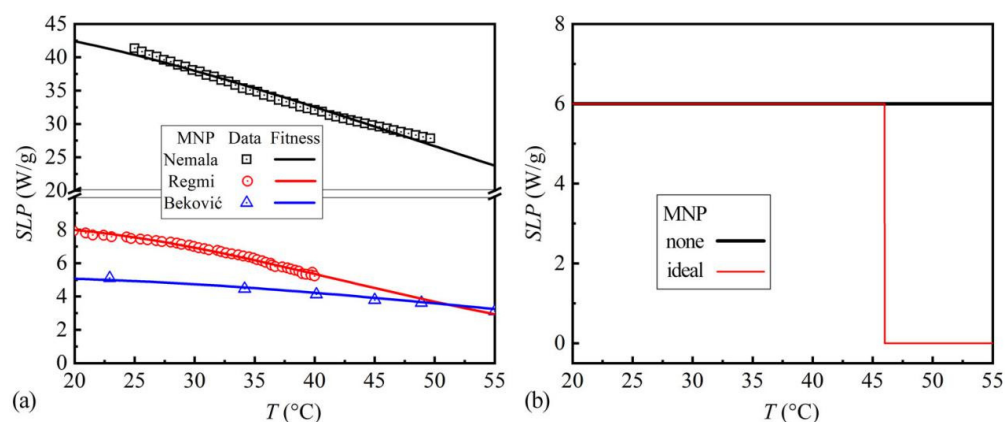


Figure 4. (a) The SLP data and fitted SLP - T curves of MNP_{Nemala} , MNP_{Regmi} , and $MNP_{Beković}$; the SLP data are obtained from the references [15–17]; (b) The SLP - T curves of MNP_{none} and MNP_{ideal} .

Table 3. Gaussian fitting parameters of SLP - T curves for the MNPs from references.

	<i>a</i>	<i>b</i>	<i>c</i>
MNP_{Nemala}	46.350	0	67.240
MNP_{Regmi}	8.257	12.480	41.810
$MNP_{Beković}$	5.158	11.240	64.400

3.2.2. Capacities

For heating capability evaluation, the proper MNP concentration for heating the tumor center to 46 °C is searched for each kind of MNP. The T_{center} s and T_{edge} s at different MNP concentrations (C_s) are shown in Figure 5a,c,e marked as envelope curves. The MNP_{none} and MNP_{ideal} in Figure 5e have the same temperature distributions below 17.39 mg/mL. Over this concentration, the temperatures of the MNP_{none} increase linearly, while the T_{center} of MNP_{ideal} self-regulates at 46 °C. The exceeded concentration only elevates the T_{edge} of MNP_{ideal} , indicating the whole tumor approaches 46 °C and the temperature distribution may be more uniform. The temperature-concentration curves of the actual MNPs, in Figure 5a,c, show upper convex shapes, indicating they have part of the self-regulating abilities. At extortionate concentrations, the T_{center} of ZnCoCrFeO MNPs with lower T_C , in Figure 5a, is closer to 46 °C, suggesting better self-regulating abilities. For the sake of comparing the heating performances of the different MNPs, the proper concentrations, providing the T_{center} of 46 °C, are chosen in Figure 5a,c and will be used in the following analysis. Since the MNP_{ideal} has a large range of concentrations for T_{center} of 46 °C, a high concentration of 100 mg/mL is selected, which can increase the T_{edge} over 42 °C. At the proper concentrations, the PDP - T curves are calculated by Equation (10) and shown in Figure 5b,d,f.

After confirming their abilities to heat the tumor to 46 °C, whether the corresponding AMF conditions and concentrations are safe still needs to be investigated. High AMF intensity or frequency may cause pain [1]. Normally, the safe criteria for AMF are “intensity (H) × frequency (f) < 5 × 10⁹ A/(m·s)” [28]. High MNP concentrations may lead to cytotoxicity [14]. The maximum ever applied MNP concentration, recorded in clinical trials, is 280 mg/mL [29]. With regards to the ZnCoCrFeO MNPs, the AMF conditions of 100 kHz and 400 Oe (32 kA/m) in calorimetry experiments and the chosen MNP concentrations of 30–95 mg/mL in Figure 5a may be acceptable. For the MNPs in Figure 5c, the chosen AMF conditions of MNP_{Nemala} (375 kHz, 11.28 kA/m) [15], MNP_{Regmi} (395 kHz, 5.6 kA/m) [16], and $MNP_{Beković}$ (100 kHz, 15 kA/m) [17], as well as the MNP concentrations of 3–27 mg/mL in Figure 5c may also be acceptable. So, these MNPs may be

capable of hyperthermia. Noticeably, the safe AMF criteria depend on the body diameter exposed to the AMF, and the acceptable MNP concentration relates to the MNP composition, the biocompatibility of the surface coating, and so on. So, the capability of the specific MNPs will need detailed evaluations in clinical applications. Overall, by simulating the temperature-dependent heating efficiencies, the required concentration of MNPs can be determined, and the safety can be discussed.

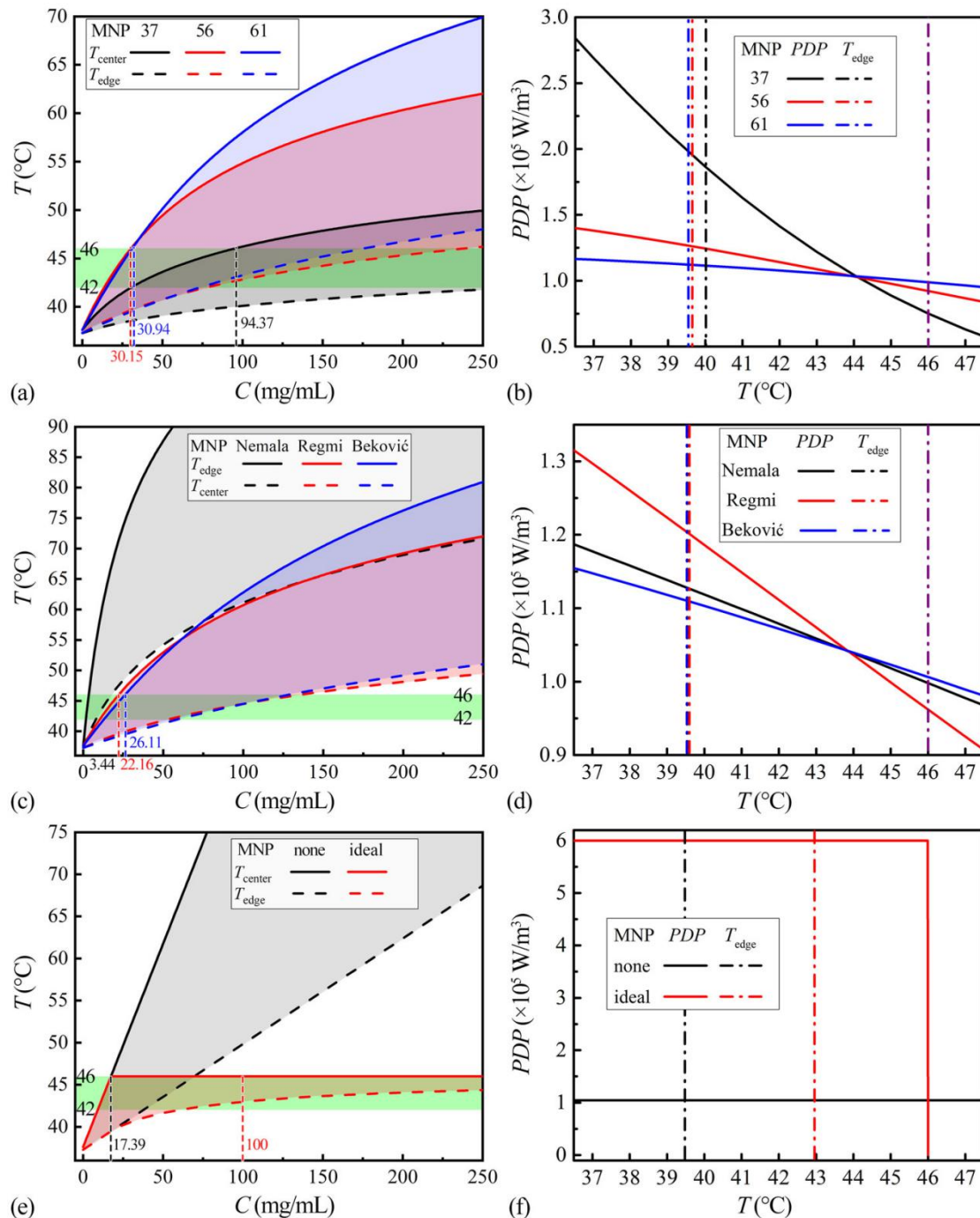


Figure 5. The temperature range ($T_{center}-T_{edge}$) at different MNP concentrations of MNP₃₇, MNP₅₆ and MNP₆₁ (a); of MNP_{Nemala}, MNP_{Regmi} and MNP_{Beković} (c); of MNP_{none} and MNP_{ideal} (e). The PDP- T curves at proper concentrations for T_{center} 46 °C of MNP₃₇, MNP₅₆ and MNP₆₁ (b); of MNP_{Nemala}, MNP_{Regmi} and MNP_{Beković} (d); of MNP_{none} and MNP_{ideal} (f).

In clinical hyperthermia applications, the AMF conditions and concentrations can be adjusted according to patient tolerance. If the patient is more sensitive to the pain, the AMF intensity needs to be reduced [1]. Consequently, the MNP concentration requires elevation for ensuring effective heating. The balance of the AMF and MNP concentration values refers to Equation (10). In Equation (10), the $PDP(T)$ equals $SLP(T) \times C$, where the SLP is proportional to the square of AMF intensity (H^2), and correlates to the AMF frequency (f), according to Rosensweig's model [30]. Thus, multiple combinations of H , f and C values can lead to the same $PDP-T$ curves in Figure 5b,d, which result in effective heating. In addition, the combination with lower overall side effects can be selected among them. For instance, if the MNPs have excellent biocompatibility, raising the concentration to four times and reducing the H to half will lower the pain risk of high AMF but still maintain the T_{center} at 46 °C.

3.2.3. Uniformities

The temperature distributions in the tumor model are shown by the radius in Figure 6a,c,e (left ordinate), and by the volume in Figure 6b,d,f (left ordinate). Along the radial direction, the temperature decreases from the center to edge. The actual MNPs (Figure 6a–d) have higher temperatures all over the tumor than the MNP_{none} (Figure 6e,f), indicating more uniform temperature distributions. In addition, the MNP_{37} has the best uniformities among the investigated actual MNPs. However, they cannot provide a temperature distribution like the MNP_{ideal} , which forms 46 °C in over half of the tumor in Figure 6f.

In clinical trials, the final temperatures at the tumor center (T_{center}) and the tumor edge (T_{edge}), as well as the exceeded temperatures in 20% volume (T_{20}), 50% volume (T_{50}), 90% volume (T_{90}) of the tumor are concerned [29]. To quantitatively evaluate the uniformities, the dimensionless parameter U_i is defined, shown in Equations (12) and (13).

$$U_i = \frac{p_i - p_i^0}{1 - p_i^0} \quad (12)$$

$$p_i = \frac{T_i - 37}{T_{center} - 37} \quad (13)$$

where, the subscript i can be 20, 50, 90 and edge, representing 20% volume, 50% volume, 90% volume of the tumor, and the tumor edge; the superscript 0 represents the values obtained from the MNP_{none} (Figure 6f). The temperature distribution of the MNP_{none} is taken as the baseline, corresponding to $U_i = 0$. Higher U_i means the temperature is closer to T_{center} . $U_i = 1$ means extremely uniform. The uniformity indexes of corresponding MNPs are shown in Figure 7a. The results suggest that the ZnCoCrFeO MNPs with lower T_C have higher uniformity at each position. The MNP_{ideal} and MNP_{none} present the upper and lower limits of uniformities. Among the actual MNPs, the MNP_{37} has the highest U_{90} , indicating the best therapeutic outcome [29,31].

The improvements in uniformity result from the equalized absorbed energies (for temperature rise) within the tumor. Before interpreting the contribution of the decreased $PDPs$ with increased temperatures in this process, the reason for the temperature distribution of “inner higher, outer lower” needs to be explained first. Taking the MNP_{none} with constant SLP as an example, when a small amount of MNPs is placed in a tumor as a unit and starts to generate heat, part of the generated heat will elevate the temperature of the local tissue, and the rest will be transferred to the ambient tissues. If three equidistant units are arranged in a line around the tumor center, the central part will receive most of the energy for temperature rise, thus higher temperature at the center. So, when the sphere tumor is uniformly filled with such units of MNP_{none} , the temperature decreases from the tumor center to the edge, as seen in Figure 6e,f. Once the SLP of MNPs decreases with the increased temperatures, the powers of the inner hot units are restricted automatically, reducing the central and overall temperatures. To maintain the same T_{center} , a higher con-

centration is needed. In addition, compensatory elevations in outer units' powers present as higher PDP s in outer regions. The phenomenon can be seen through the PDP - T curves of the actual MNPs and MNP_{ideal} in Figure 6 (right ordinate). Thus, the MNPs with steeper PDP - T curves form more uneven PDP distributions with higher values around the tumor center, helping to equalize the absorbed energies in different regions and leading to better temperature uniformity.

The uniformity improvement can also be accomplished by distributing more MNPs around the tumor center, regardless of the T_C . Bagaria, et al. simulated different secondary polynomial MNPs' radial distributions [32]. Liangruksa, et al. compared the homogenous, exponential, and Gaussian MNP distributions [33]. Zhang, et al. divided the tumor into multi regions with different MNP concentrations [34]. They all proved that, by distributing more MNPs around the tumor center patterns, the PDP at the center is higher, leading to more uniform temperature distributions. So, the temperature uniformities of the MNPs with low T_C can be further improved by optimizing the distribution of the MNPs in the tumor.

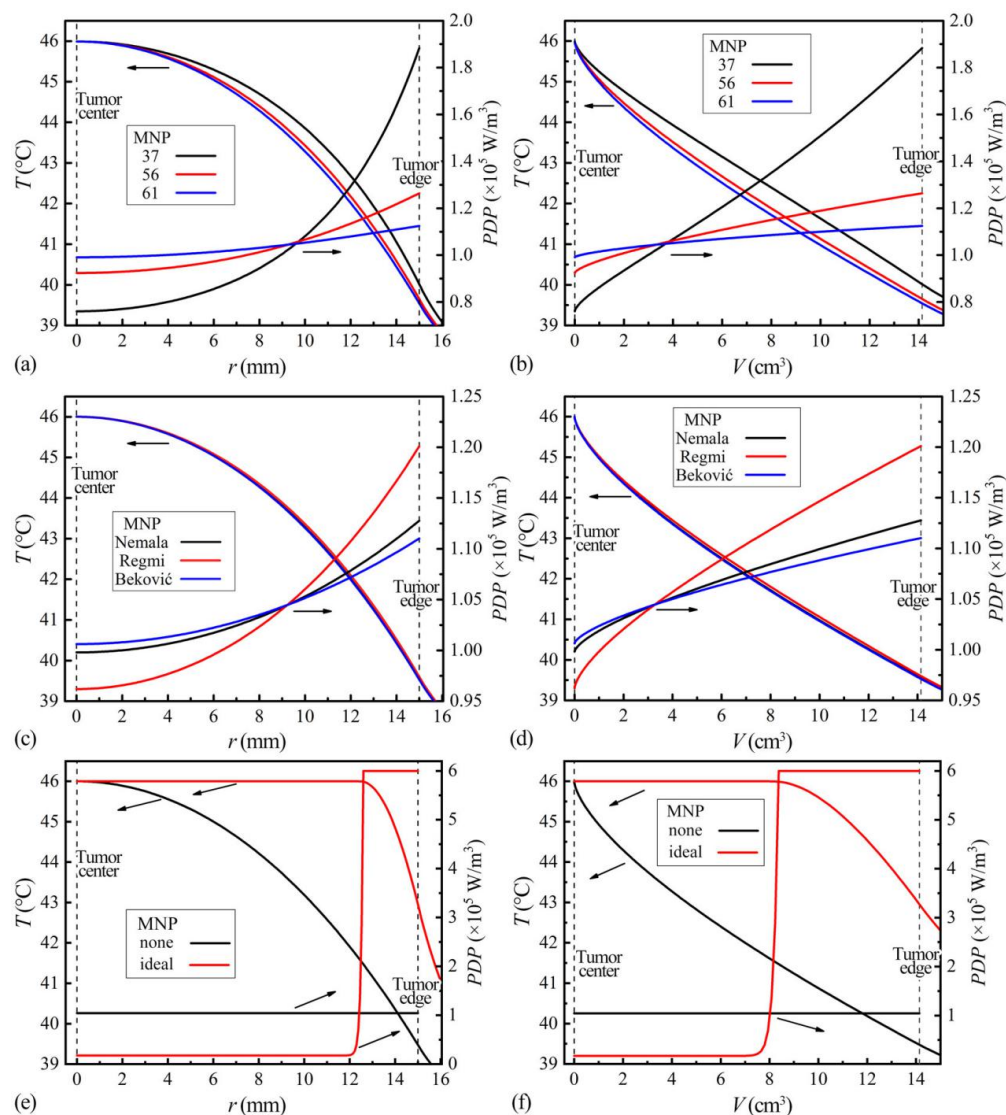


Figure 6. Temperature distributions (left ordinate) and PDP distributions (right ordinate) in the tumor of the $ZnCoCrFeO$ MNPs by radius (a), by volume (b); of the MNPs from references by radius (c), by volume (d); and of the MNP_{ideal} and MNP_{none} by radius (e), by volume (f).

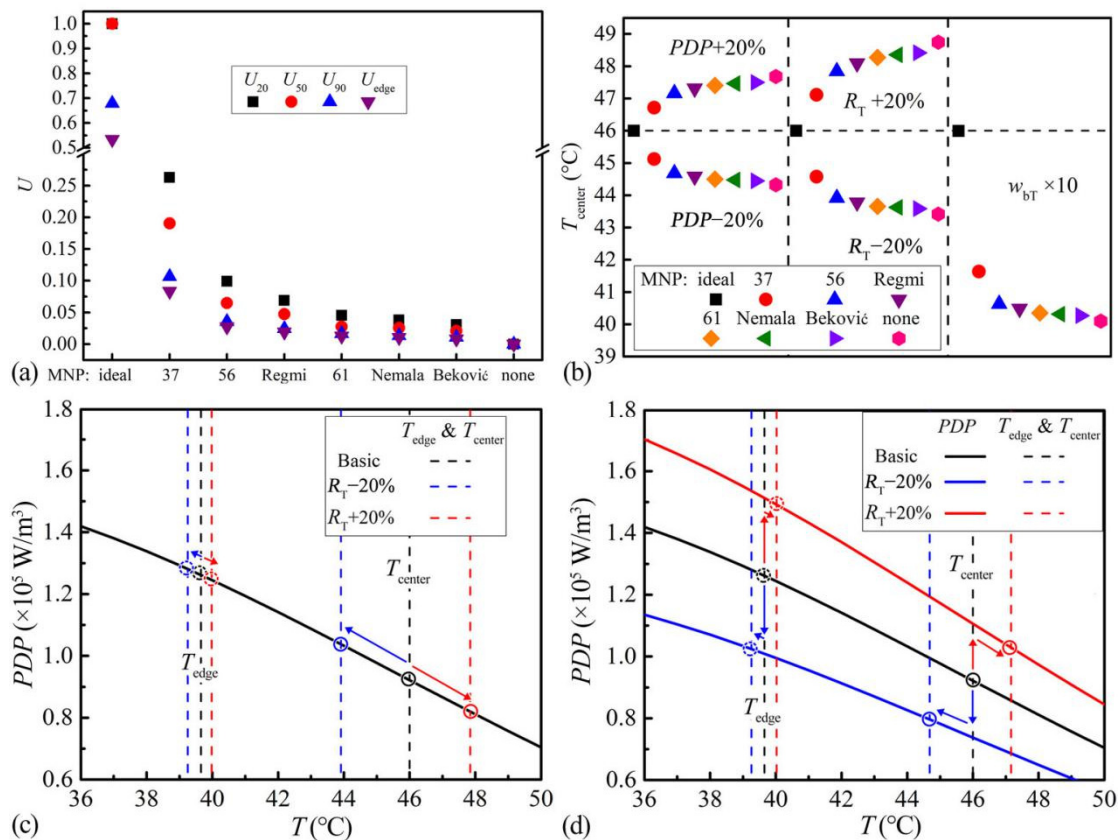


Figure 7. (a) Temperature uniformities (U) of the ZnCoCrFeO MNPs, the MNPs from references, MNP_{ideal} and MNP_{none} . (b) Stabilities (T_{center} changes) under PDP , R_T and w_{bT} fluctuations of the ZnCoCrFeO MNPs, the MNPs from references, MNP_{ideal} and MNP_{none} ; (c) Changes of temperature ranges of the MNP_{56} under R_T fluctuations; (d) Changes of temperature ranges and PDP - T curves of the MNP_{56} under PDP fluctuations.

3.2.4. Stabilities

In hyperthermia of MNPs, the reasons for temperature instabilities can be summed up as the changes of heat sources (heat generation) and the tumor properties (heat dissipation). (a) For heat sources, the AMF and the concentration influence heat generation. In clinical trials, the applied AMF intensity and frequency may fluctuate, influencing the SLP of MNPs [1,29]. Furthermore, the concentrations of MNPs may change in the subsequent therapeutic procedure. For instance, in a tumor mouse model, only 3/4 of the applied MNPs can be detected after 24 h [35]. Thus, the PDP of the heat source may be affected by the SLP and concentration (Equation (10)), altering the temperature distribution in the tumor. (b) For tumor properties, the tumor itself may progress or recover, affecting the heating process. The alteration of tumor size (R_T) affects the heat dissipation efficiency from tumor to peripheral tissue. Larger R_T provides a smaller surface area over volume ratio, leading to more heat retention and higher temperatures in the tumor. Besides, the blood perfusion rate in tumors (w_{bT}), which relates to heat dissipation along blood vessels, varies with the tumor stages and also impacts the temperature distribution significantly [36]. So, the varying PDP , R_T and w_{bT} mainly contribute to the instability of hyperthermia.

For evaluating the stabilities of MNPs, the simulations with the T_{center} of 46 °C in Figure 5 are taken as the base. The PDP , R_T in Equation (2) and w_{bT} in Equation (9) are separately changed in the simulations and the resultant changes in T_{center} are compared as stability evaluations, as shown in Figure 7b. For the influences of heat source change, 20% increase and decrease of PDP are simulated. For the impact of tumor progression or recovery, 20% increase and decrease of R_T are simulated. For the effect of tumor blood system recovery, 10 times of w_{bT} is simulated in reference to the w_{bT} range of liver

($0.000833\text{--}0.02289\text{ s}^{-1}$) [26]. In the results, less change in T_{center} (closer to $46\text{ }^{\circ}\text{C}$) represents better stability. The increases of PDP and R_T cause overheating. The decreases of PDP and R_T , as well as the elevation of w_{bT} , lead to insufficient heating. The changes of T_{center} are less for the ZnCoCrFeO MNPs with lower T_C , indicating higher stabilities. The actual MNPs are better than the MNP_{none} . The $\text{MNP}_{\text{ideal}}$ can self-regulate the T_{center} at $46\text{ }^{\circ}\text{C}$ for all situations.

The improvements of stabilities result from the automatic adaptation of PDP s to the thermal parameter fluctuations. However, the PDP behaviors for alleviating the fluctuations from the environment and the heat source are different. (a) For the fluctuations in the heat dissipation environment, the R_T and w_{bT} alterations are included. Taking R_T fluctuations of MNP_{56} as examples, the PDP - T curve and original temperature range (T_{center} and T_{edge}) are drawn in Figure 7c. When the temperature decreases, the temperature range in Figure 7c shifts lower (blue dash lines), while the PDP - T curve remains unchanged (black solid line). At this time, the PDP s of all units in the tumor increase with the shifted temperature range, causing an elevation of the overall PDP in the tumor (blue circles), thus alleviating the effect of the environmental changes and exhibiting self-regulating behaviors. (b) For the fluctuations in the heat source, the PDP alteration is included. Taking the MNP_{56} as an example, the PDP - T curve and original temperature range are drawn in Figure 7d. When the PDP s of all units decrease (blue solid line), the temperature ranges also decrease (blue dash lines), elevating the units' PDP s back a little bit (blue circles). Thus, for both situations, although the mechanisms are different, a steeper PDP - T curve always leads to better stabilities. In addition, the MNP_{37} has the steepest PDP - T curve and the best stabilities among the actual MNPs.

The simulation methods on stability established here can quantitatively evaluate the MNPs' abilities of self-regulating temperatures. Unlike the uniformities, stability superiority cannot be achieved by properly distributing the MNPs but may be approached by monitoring the temperatures in the tumor and adjusting the intensity and frequency of AMF. Besides, sifting the MNPs with the same T_C helps to gather the MNPs with the same SLP decrease temperature and may offer the MNPs steeper PDP - T curves, thus improving the stabilities. The evaluation methods, proposed in this paper, are applicable to other kinds of tumors with different shapes, as well as hyperthermia with different temperature ranges, such as $46\text{--}60\text{ }^{\circ}\text{C}$.

4. Conclusions

A simulation method for quantitatively evaluating the heating performances of MNPs is established here. By simulating the temperature-dependent SLP of MNPs, evaluations on the heating capacity, uniformity, and stability can be performed. Through the applications of the method on the ZnCoCrFeO, Fe_3O_4 and $\gamma\text{-Fe}_2\text{O}_3$ MNPs, it can be seen that, with proper concentrations, these MNPs are capable of $46\text{ }^{\circ}\text{C}$ hyperthermia for the proposed tumor model. Moreover, the MNPs with steeper PDP - T curves within $37\text{--}46\text{ }^{\circ}\text{C}$ have better uniformities and stabilities, relying on restricting the PDP around the tumor center and automatically regulating the PDP under temperature change.

Author Contributions: Conceptualization, S.-W.D., C.-W.W. and W. Z.; methodology, S.-W.D.; software, S.-W.D.; validation, C.D. formal analysis, S.-W.D.; investigation, S.-W.D.; resources, S.-W.D.; data curation, S.-W.D. and C.D.; writing—original draft, S.-W.D.; writing—review & editing, X.-G.Y., W.Z. and J.-P.G.; visualization, S.-W.D.; supervision, C.-W.W. and W.Z.; project administration, W.Z.; funding acquisition, W.Z.. All authors have read and agreed to the published version of the manuscript.

Funding: This work was supported by the National Key R&D Project of China (2018YFA0704103, 2018YFA0704104), National Natural Science Foundation China (12172083, U1908233), and Fundamental Research Funds for the Central Universities (DUT21TD105).

Institutional Review Board Statement: Not applicable.

Informed Consent Statement: Not applicable.

Data Availability Statement: The data that support the findings of this study are available from the corresponding author upon reasonable request.

Conflicts of Interest: The authors declare no conflict of interest.

Abbreviations

AMF	alternating magnetic field
T_C	Curie temperature ($^{\circ}\text{C}$)
MHG	magnetic hydrogel
MNP	magnetic nanoparticles
MNP ₃₇ , MNP ₅₆ , MNP ₆₁	ZnCoCrFeO MNPs with T_C of 37.5 $^{\circ}\text{C}$, 56.0 $^{\circ}\text{C}$ and 61.0 $^{\circ}\text{C}$
MNP _{Nemala}	MNPs by Nemala et al.
MNP _{Regmi}	MNPs by Regmi et al.
MNP _{Beković}	MNPs by Beković et al.
MNP _{ideal}	assumed ideal MNPs with T_C of 46 $^{\circ}\text{C}$ (heating efficiency is constant below T_C and zero above T_C)
MNP _{none}	assumed MNPs without T_C (heating efficiency does not change with temperature)
b (subscript)	of blood
L (subscript)	of healthy liver tissue
MHG (subscript)	of MHG
MNP (subscript)	of MNPs
T (subscript)	of tumor
TP (subscript)	of tumor and MNPs
T ($^{\circ}\text{C}$)	temperature
t (s)	time
T_{center} ($^{\circ}\text{C}$)	temperature at the center of the tumor
T_{20} , T_{50} , T_{90} ($^{\circ}\text{C}$)	temperatures exceeded in 20%, 50% or 90% volume of the tumor
T_{edge} ($^{\circ}\text{C}$)	temperature at the edge between tumor and healthy tissue
T_{α} ($^{\circ}\text{C}$)	the temperature of arterial blood (37 $^{\circ}\text{C}$)
U_{20} , U_{50} , U_{90} , U_{edge} (dimensionless)	uniformities within 20%, 50%, 90% or 100% volume of the tumor
SLP (W/g)	specific loss power
PDP (W/m ³)	power dissipation of MNPs per unit of tumor volume
c (J/(kg $\cdot^{\circ}\text{C}$))	specific heat capacity
C (kg/m ³ or mg/mL)	MNP concentration in tumor region (MNP mass/tumor volume)
R_T , R_L (mm)	radiuses of tumor region and overall healthy liver region
r (mm)	radius from the tumor center
ρ (kg/m ³)	density
k (W/(m $\cdot^{\circ}\text{C}$))	thermal conductivity
Q_m (W/m ³)	power density of metabolic heat generation
Q_{m0} (W/m ³)	power density of metabolic heat generation at body temperature (37 $^{\circ}\text{C}$)
Q_b (W/m ³)	power density of heat dissipation by blood perfusion effect
w_b (1/s)	blood perfusion rate
ϕ	volume fraction of MNPs in the tumor

References

- Johannsen, M.; Gneveckow, U.; Eckelt, L.; Feussner, A.; Waldöfner, N.; Scholz, R.; Deger, S.; Wust, P.; Loening, S.A.; Jordan, A. Clinical hyperthermia of prostate cancer using magnetic nanoparticles: Presentation of a new interstitial technique. *Int. J. Hyperther.* **2005**, *21*, 637–647. [[CrossRef](#)] [[PubMed](#)]
- Wust, P.; Gneveckow, U.; Johannsen, M.; Böhmer, D.; Henkel, T.; Kahmann, F.; Sehouli, J.; Felix, R.; Rieke, J.; Jordan, A. Magnetic nanoparticles for interstitial thermotherapy—feasibility, tolerance and achieved temperatures. *Int. J. Hyperther.* **2006**, *22*, 673–685. [[CrossRef](#)] [[PubMed](#)]
- Maier-Hauff, K.; Ulrich, F.; Nestler, D.; Niehoff, H.; Wust, P.; Thiesen, B.; Orawa, H.; Budach, V.; Jordan, A. Efficacy and safety of intratumoral thermotherapy using magnetic iron-oxide nanoparticles combined with external beam radiotherapy on patients with recurrent glioblastoma multiforme. *J. Neuro-Oncol.* **2011**, *103*, 317–324. [[CrossRef](#)] [[PubMed](#)]

4. Grauer, O.; Jaber, M.; Hess, K.; Weckesser, M.; Schwindt, W.; Maring, S.; Wölfer, J.; Stummer, W. Combined intracavitary thermotherapy with iron oxide nanoparticles and radiotherapy as local treatment modality in recurrent glioblastoma patients. *J. Neuro-Oncol.* **2019**, *141*, 83–94. [[CrossRef](#)]
5. Yu, X.; Ding, S.; Yang, R.; Wu, C.; Zhang, W. Research progress on magnetic nanoparticles for magnetic induction hyperthermia of malignant tumor. *Ceram. Int.* **2021**, *47*, 5909–5917. [[CrossRef](#)]
6. Astefanoaei, I.; Dumitru, I.; Chiriac, H.; Stancu, A. Controlling temperature in magnetic hyperthermia with low Curie temperature particles. *J. Appl. Phys.* **2014**, *115*, 17B531. [[CrossRef](#)]
7. Tang, Y.-D.; Flesch, R.; Jin, T. Numerical analysis of temperature field improvement with nanoparticles designed to achieve critical power dissipation in magnetic hyperthermia. *J. Appl. Phys.* **2017**, *122*, 034702. [[CrossRef](#)]
8. Prasad, N.K.; Rathinasamy, K.; Panda, D.; Bahadur, D. T_C -tuned biocompatible suspension of $\text{La}_{0.73}\text{Sr}_{0.27}\text{MnO}_3$ for magnetic hyperthermia. *J. Biomed. Mater. Res. B* **2008**, *85B*, 409–416. [[CrossRef](#)]
9. Hanini, A.; Lartigue, L.; Gavard, J.; Kacem, K.; Wilhelm, C.; Gazeau, F.; Chau, F.; Ammar, S. Zinc substituted ferrite nanoparticles with $\text{Zn}_{0.9}\text{Fe}_{2.1}\text{O}_4$ formula used as heating agents for in vitro hyperthermia assay on glioma cells. *J. Magn. Magn. Mater.* **2016**, *416*, 315–320. [[CrossRef](#)]
10. Yu, X.; Yang, R.; Wu, C.; Zhang, W. Effect of chromium ion substitution of ZnCo ferrites on magnetic induction heating. *J. Alloys Compd.* **2020**, *830*, 154724. [[CrossRef](#)]
11. Tang, Q.; Zhang, D.; Cong, X.; Wan, M.; Jin, L. Using thermal energy produced by irradiation of Mn-Zn ferrite magnetic nanoparticles (MZF-NPs) for heat-inducible gene expression. *Biomaterials* **2008**, *29*, 2673–2679. [[CrossRef](#)]
12. Saito, H.; Mitobe, K.; Ito, A.; Sugawara, Y.; Maruyama, K.; Minamiya, Y.; Motoyama, S.; Yoshimura, N.; Ogawa, J. Self-regulating hyperthermia induced using thermosensitive ferromagnetic material with a low Curie temperature. *Cancer Sci.* **2008**, *99*, 805–809. [[CrossRef](#)] [[PubMed](#)]
13. Ito, A.; Saito, H.; Mitobe, K.; Minamiya, Y.; Takahashi, N.; Maruyama, K.; Motoyama, S.; Katayose, Y.; Ogawa, J.-I. Inhibition of heat shock protein 90 sensitizes melanoma cells to thermosensitive ferromagnetic particle-mediated hyperthermia with low Curie temperature. *Cancer Sci.* **2009**, *100*, 558–564. [[CrossRef](#)] [[PubMed](#)]
14. Ding, S.; Wu, C.-W.; Yu, X.-G.; Li, H.; Yu, L.; Zhang, Y.-X.; Yang, R.-P.; Zhang, W. Magnetic hydrogel with long *in situ* retention time for self-regulating temperature hyperthermia. *Int. J. Hyperth.* **2021**, *38*, 13–21. [[CrossRef](#)] [[PubMed](#)]
15. Nemala, H.; Thakur, J.S.; Naik, V.M.; Vaishnava, P.P.; Lawes, G.; Naik, R. Investigation of magnetic properties of Fe_3O_4 nanoparticles using temperature dependent magnetic hyperthermia in ferrofluids. *J. Appl. Phys.* **2014**, *116*, 034309. [[CrossRef](#)]
16. Regmi, R.; Naik, A.; Thakur, J.S.; Vaishnava, P.P.; Lawes, G. Temperature dependent dissipation in magnetic nanoparticles. *J. Appl. Phys.* **2014**, *115*, 17B301. [[CrossRef](#)]
17. Beković, M.; Trlep, M.; Jesenik, M.; Goričan, V.; Hamler, A. An experimental study of magnetic-field and temperature dependence on magnetic fluid's heating power. *J. Magn. Magn. Mater.* **2013**, *331*, 264–268. [[CrossRef](#)]
18. Hilger, I.; Frühauf, K.; Andrá, W.; Hiergeist, R.; Hergt, R.; Kaiser, W.A. Heating potential of iron oxides for therapeutic purposes in interventional radiology. *Acad. Radiol.* **2002**, *9*, 198–202. [[CrossRef](#)]
19. Bordelon, D.E.; Cornejo, C.; Grüttner, C.; Westphal, F.; DeWeese, T.L.; Ivkov, R. Magnetic nanoparticle heating efficiency reveals magneto-structural differences when characterized with wide ranging and high amplitude alternating magnetic fields. *J. Appl. Phys.* **2011**, *109*, 124904. [[CrossRef](#)]
20. Wildeboer, R.R.; Southern, P.; Pankhurst, Q.A. On the reliable measurement of specific absorption rates and intrinsic loss parameters in magnetic hyperthermia materials. *J. Phys. D Appl. Phys.* **2014**, *47*, 495003. [[CrossRef](#)]
21. Ebrahimi, M. On the temperature control in self-controlling hyperthermia therapy. *J. Magn. Magn. Mater.* **2016**, *416*, 134–140. [[CrossRef](#)]
22. Astefanoaei, I.; Dumitru, I.; Chiriac, H.; Stancu, A. Thermo-fluid analysis in magnetic hyperthermia using low Curie temperature particles. *IEEE Trans. Magn.* **2016**, *52*, 1–5. [[CrossRef](#)]
23. Wang, Q.; Deng, Z.S.; Liu, J. Theoretical evaluations of magnetic nanoparticle-enhanced heating on tumor embedded with large blood vessels during hyperthermia. *J. Nanopart. Res.* **2012**, *14*, 974. [[CrossRef](#)]
24. Gupta, P.K.; Singh, J.; Rai, K.N. Numerical simulation for heat transfer in tissues during thermal therapy. *J. Therm. Biol.* **2010**, *35*, 295–301. [[CrossRef](#)]
25. Pennes, H.H. Analysis of tissue and arterial blood temperatures in the resting human forearm. *J. Appl. Physiol.* **1948**, *1*, 93–122. [[CrossRef](#)]
26. Hasgall, P.A.; Di Gennaro, F.; Baumgartner, C.; Neufeld, E.; Lloyd, B.; Gosselin, M.C.; Payne, D.; Klingeböck, A.; Kuster, N. *IT'IS Database for Thermal and Electromagnetic Parameters of Biological Tissues, Version 4.0*; IT'IS Foundation: Zurich, Switzerland, 2018.
27. Raouf, I.; Khalid, S.; Khan, A.; Lee, J.; Kim, H.S.; Kim, M.-H. A review on numerical modeling for magnetic nanoparticle hyperthermia: Progress and challenges. *J. Therm. Biol.* **2020**, *91*, 102644. [[CrossRef](#)]
28. Hergt, R.; Dutz, S. Magnetic particle hyperthermia-biophysical limitations of a visionary tumour therapy. *J. Magn. Magn. Mater.* **2007**, *311*, 187–192. [[CrossRef](#)]
29. Johannsen, M.; Gneveckow, U.; Thiesen, B.; Taymoorian, K.; Cho, C.H.; Waldöfner, N.; Scholz, R.; Jordan, A.; Loening, S.A.; Wust, P. Thermotherapy of prostate cancer using magnetic nanoparticles: Feasibility, imaging, and three-dimensional temperature distribution. *Eur. Urol.* **2006**, *52*, 1653–1662. [[CrossRef](#)]
30. Rosensweig, R.E. Heating magnetic fluid with alternating magnetic field. *J. Magn. Magn. Mater.* **2002**, *252*, 370–374. [[CrossRef](#)]

31. Thrall, D.E.; Rosner, G.L.; Azuma, C.; LaRue, S.M.; Case, B.C.; Samulski, T.; Dewhurst, M.W. Using units of CEM 43 °C T_{90} , local hyperthermia thermal dose can be delivered as prescribed. *Int. J. Hyperth.* **2000**, *16*, 415–428. [[CrossRef](#)]
32. Bagaria, H.G.; Johnson, D.T. Transient solution to the bioheat equation and optimization for magnetic fluid hyperthermia treatment. *Int. J. Hyperth.* **2005**, *21*, 57–75. [[CrossRef](#)] [[PubMed](#)]
33. Liangruksa, M.; Ganguly, R.; Puri, I.K. Parametric investigation of heating due to magnetic fluid hyperthermia in a tumor with blood perfusion. *J. Magn. Magn. Mater.* **2011**, *323*, 708–716. [[CrossRef](#)]
34. Zhang, C.; Johnson, D.T.; Brazel, C.S. Numerical study on the multi-region bio-heat equation to model magnetic fluid hyperthermia (MFH) using low Curie temperature nanoparticles. *IEEE Trans. Nanobiosci.* **2008**, *7*, 267–275. [[CrossRef](#)]
35. Richter, H.; Kettering, M.; Wiekhorst, F.; Steinhoff, U.; Hilger, I.; Trahms, L. Magnetorelaxometry for localization and quantification of magnetic nanoparticles for thermal ablation studies. *Phys. Med. Biol.* **2010**, *55*, 623–633. [[CrossRef](#)] [[PubMed](#)]
36. Rast, L.; Harrison, J.G. Computational modeling of electromagnetically induced heating of magnetic nanoparticle materials for hyperthermic cancer treatment. *PIERS Online* **2010**, *6*, 5. [[CrossRef](#)]